

Supporting information for

Constructing high-performance 3D porous self-standing electrodes with various morphologies and shapes by a flexible phase separation-derived method

Hongming Yi^{a,b}, Dan Li^{a,b}, Zhiqiang Lv^{a,b}, Rui Li^{a,b}, Moxiang Ling^{a,b}, Huamin

Zhang^{a,c}, Qiong Zheng^{*a}, Xianfeng Li^{*a,c}

^aDivision of energy storage, Dalian National Laboratory for Clean Energy, Dalian Institute of Chemical Physics, Chinese Academy of Sciences, Zhongshan Road 457, Dalian 116023, P. R. China.

^bUniversity of Chinese Academy of Sciences, Beijing 100039, P. R. China.

^cCollaborative Innovation Center of Chemistry for Energy Materials (iChEM), Dalian 116023, P. R. China.

* Email: Prof. Dr. Xianfeng Li: lixianfeng@dicp.ac.cn;

Dr. Qiong Zheng: zhengqiong@dicp.ac.cn.

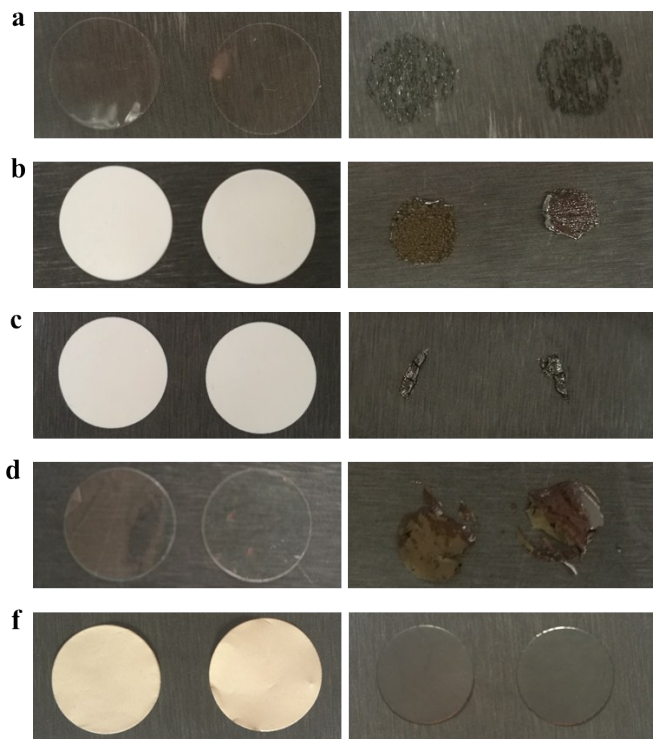


Figure S1. Digital photo of various membranes before calcination (left) and after calcination (right) at 750 °C for 4h in Ar atmosphere. (a) Nafion membrane. (b) polyether sulfone membrane (PES). (c) Polyetherimide membrane (PEI). (d) Sulfonated polyetheretherketone (SPEEK). (e) polybenzimidazole membrane (PBI).

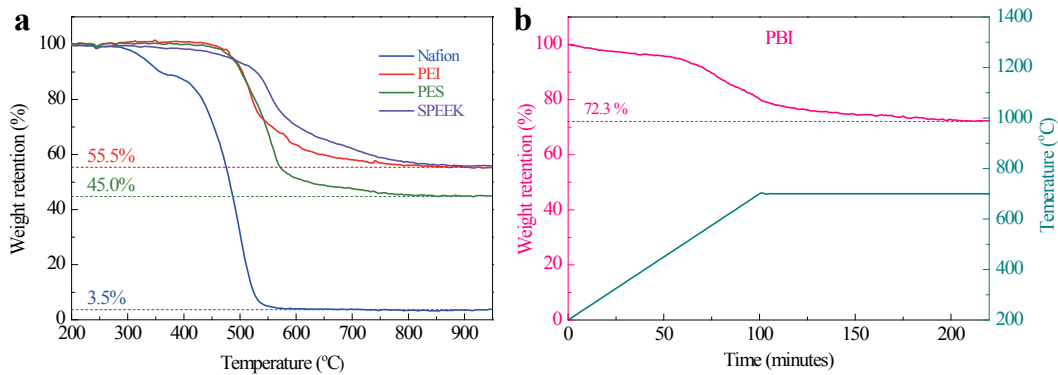


Figure S2. Thermogravimetry curves of various membranes. (a) Nafion, PES (Polyethersulfone), PEI (Polyetherimide) and Speek (Sulfonated polyetheretherketone) membranes. (b) PBI (polybenzimidazole) membrane.

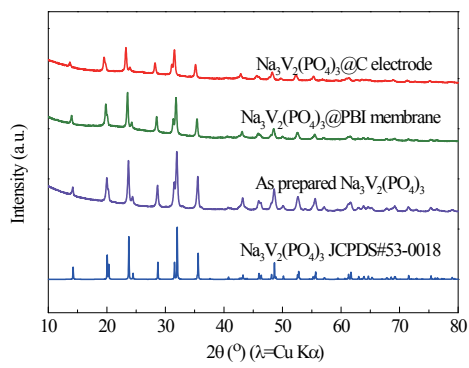


Figure S3. X-ray diffraction(XRD) patterns of as prepared $\text{Na}_3\text{V}_2(\text{PO}_4)_3$, $\text{Na}_3\text{V}_2(\text{PO}_4)_3@\text{PBI}$ membrane and $\text{Na}_3\text{V}_2(\text{PO}_4)_3@\text{C}$ electrode from ethanol induced phase separation.

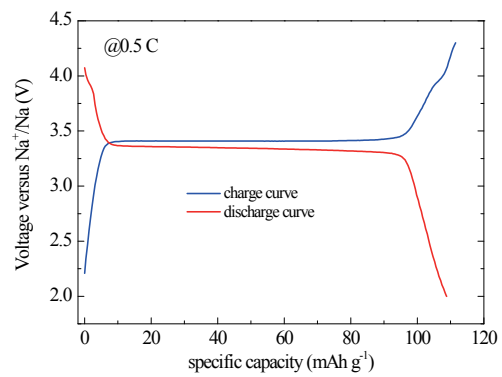


Figure S4. Galvanostatic charge-discharge curves of $\text{Na}_3\text{V}_2(\text{PO}_4)_3@\text{C}$ electrode (glass surface) from ethanol induced phase separation.

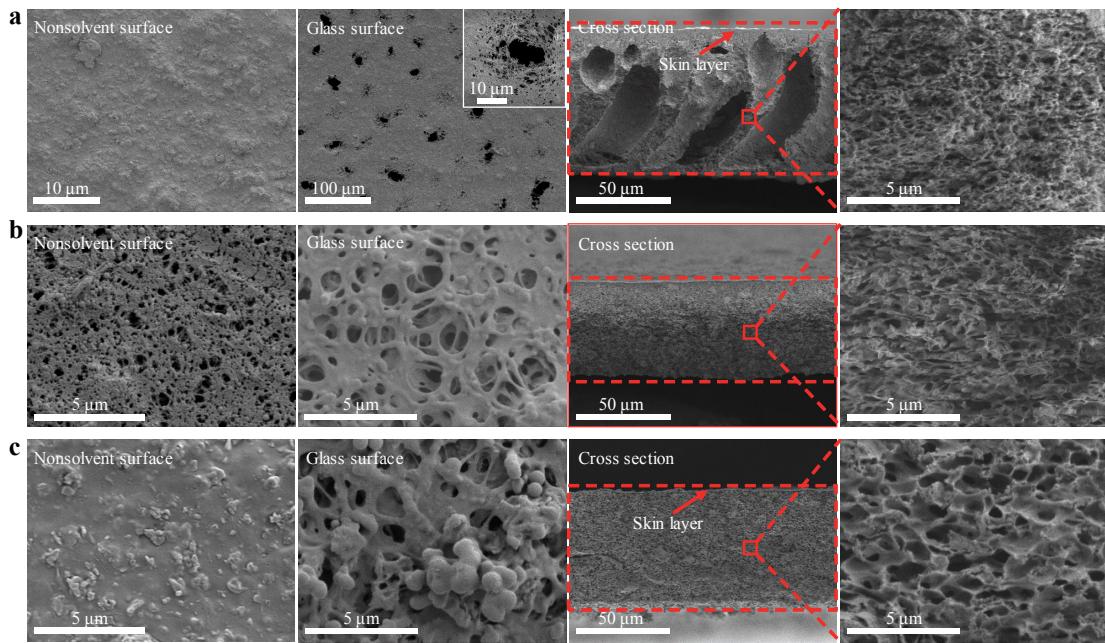


Figure S5. SEM images of self-standing $\text{Na}_3\text{V}_2(\text{PO}_4)_3@\text{PBI}$ membranes. (a) water induced phase separation. (b) ethanol induced phase separation. (c) vapor induced phase separation.

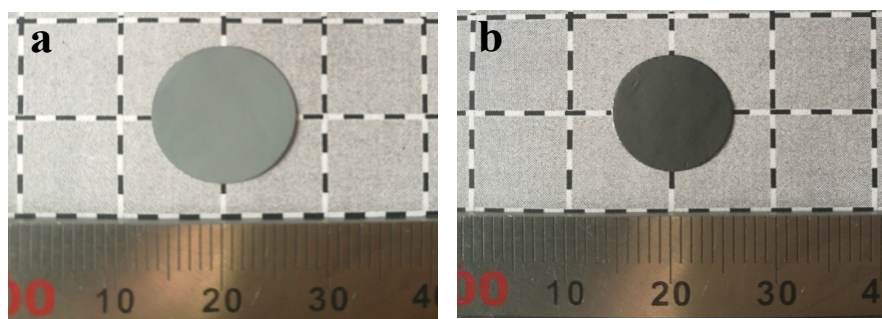


Figure S6. Digital photo of $\text{Na}_3\text{V}_2(\text{PO}_4)_3@\text{PBI}$ membrane (a) and $\text{Na}_3\text{V}_2(\text{PO}_4)_3@\text{C}$ electrode (b) with PBI: $\text{Na}_3\text{V}_2(\text{PO}_4)_3=1:1$ from ethanol induced phase separation.

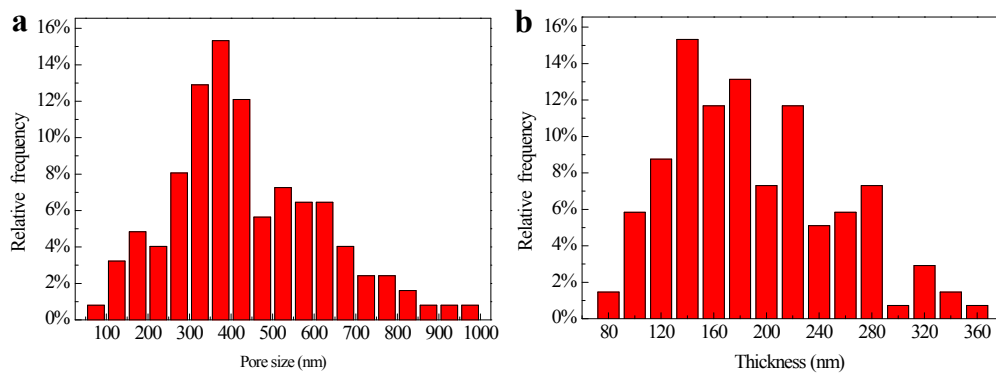


Figure S7. Pore size distribution (a) and thickness distribution of pore wall (b) of the cross section for $\text{Na}_3\text{V}_2(\text{PO}_4)_3@\text{C}$ $\text{Na}_3\text{V}_2(\text{PO}_4)_3@\text{C}$ electrode with PBI: $\text{Na}_3\text{V}_2(\text{PO}_4)_3=1:1$ from ethanol induced phase separation.

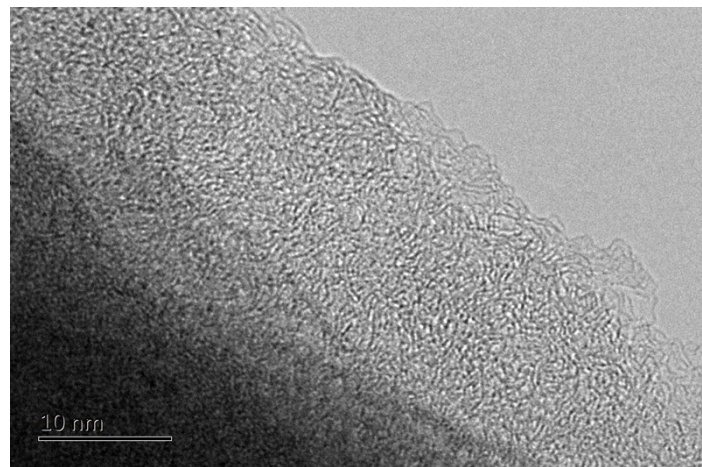


Figure S8. TEM images of $\text{Na}_3\text{V}_2(\text{PO}_4)_3@\text{C}$ electrode with PBI: $\text{Na}_3\text{V}_2(\text{PO}_4)_3=1:1$ from ethanol induced phase separation.

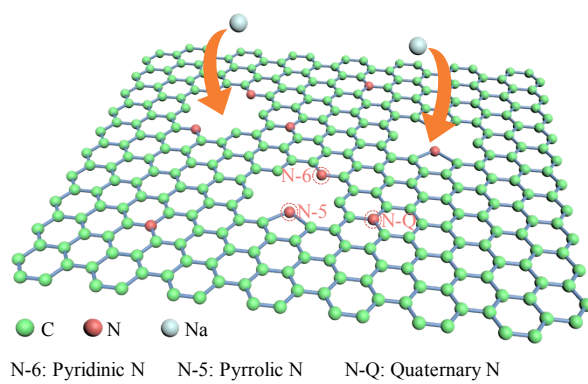


Figure S9. A schematic illustrating the structure of the N-doping species and Na^+ transporting through the graphene layer.

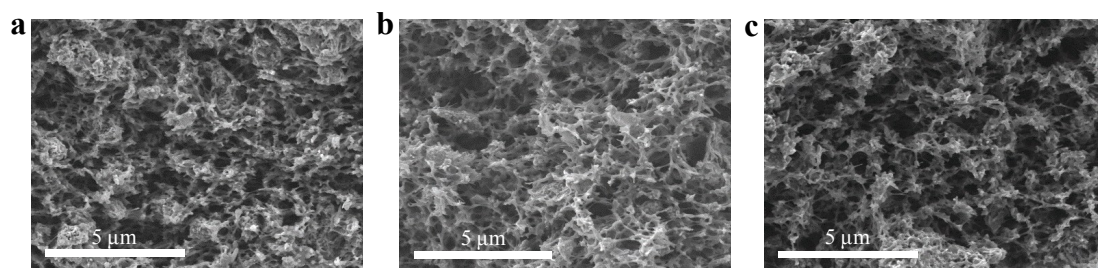


Figure S10. SEM images of $\text{Na}_3\text{V}_2(\text{PO}_4)_3@\text{C}$ electrodes (cross) section from ethanol induced phase separation. (a) PBI: $\text{Na}_3\text{V}_2(\text{PO}_4)_3=1:2$. (b) PBI: $\text{Na}_3\text{V}_2(\text{PO}_4)_3=1:3$. (c) PBI: $\text{Na}_3\text{V}_2(\text{PO}_4)_3=1:4$.

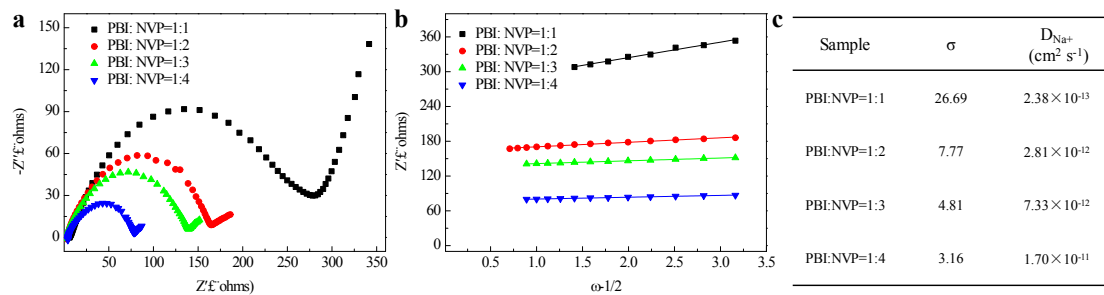


Figure S11. EIS of $\text{Na}_3\text{V}_2(\text{PO}_4)_3@\text{C}$ electrodes from ethanol phase separation-derived method with different ratio of PBI and $\text{Na}_3\text{V}_2(\text{PO}_4)_3$ (NVP). (a) The Nyquist plots. (b) The fitting equivalent circuit model for EISs. (c) The table of obtained Warburg factor (σ) and diffusion coefficient (D_{Na^+}).

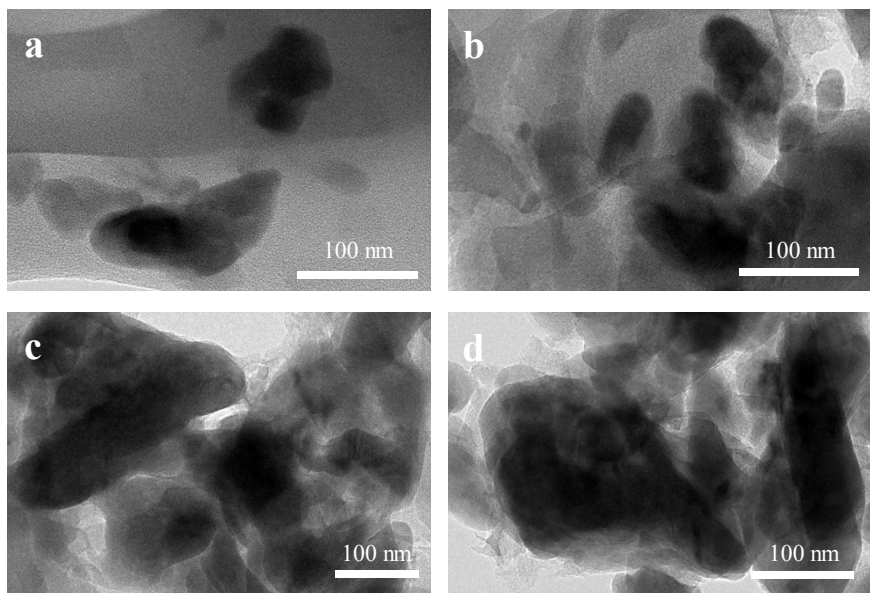


Figure S12. TEM images of $\text{Na}_3\text{V}_2(\text{PO}_4)_3@\text{C}$ electrodes. (a) PBI: $\text{Na}_3\text{V}_2(\text{PO}_4)_3=1:1$. (b) PBI: $\text{Na}_3\text{V}_2(\text{PO}_4)_3=1:2$. (c) PBI: $\text{Na}_3\text{V}_2(\text{PO}_4)_3=1:3$. (d) PBI: $\text{Na}_3\text{V}_2(\text{PO}_4)_3=1:4$.

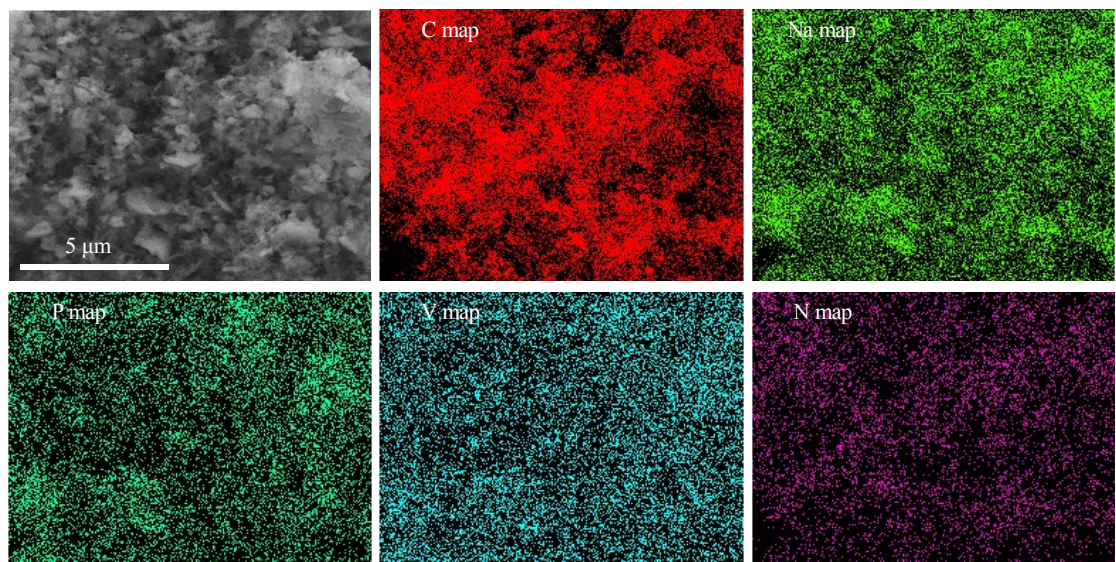


Figure S13. EDS mapping of the $\text{Na}_3\text{V}_2(\text{PO}_4)_3@\text{C}$ electrode with PBI:
 $\text{Na}_3\text{V}_2(\text{PO}_4)_3=1:2$.

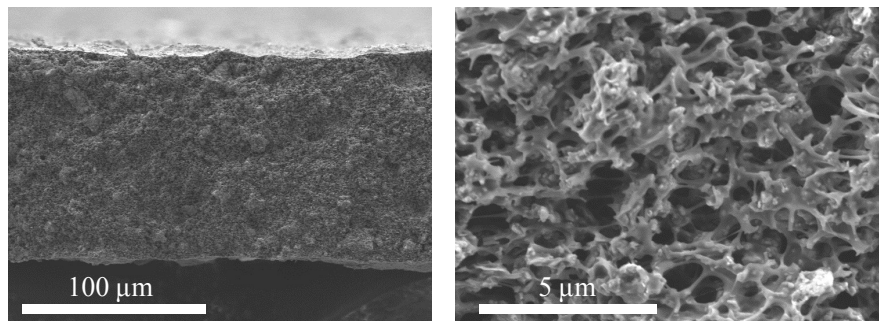


Figure S14. SEM images of the cross section for high mass loading ($\sim 6.5 \text{ mg cm}^{-2}$)

Na₃V₂(PO₄)₃@C electrode.

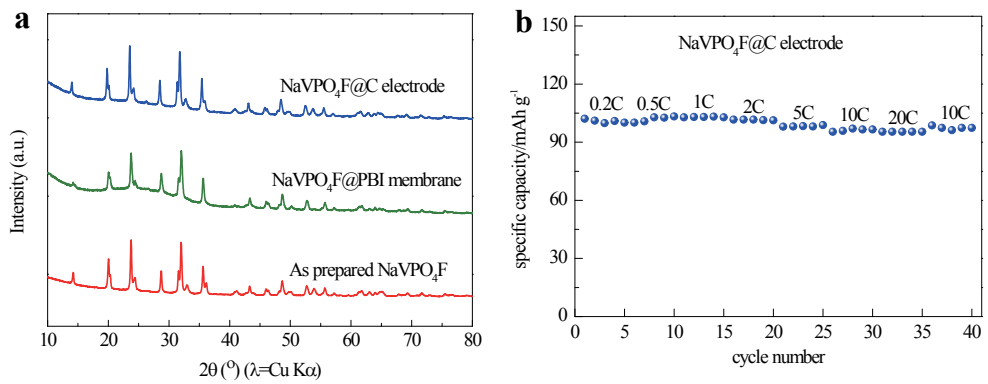


Figure S15. NaVPO₄F@C electrode. (a) X-ray diffraction (XRD) patterns. (b) Rate capability.

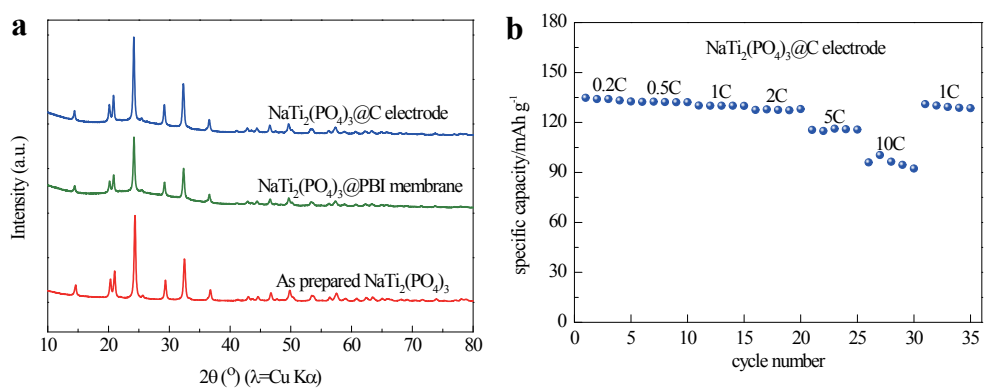


Figure S16. $\text{NaTi}_2(\text{PO}_4)_3@\text{C}$ electrode. (a) X-ray diffraction (XRD) patterns. (b) Rate capability.

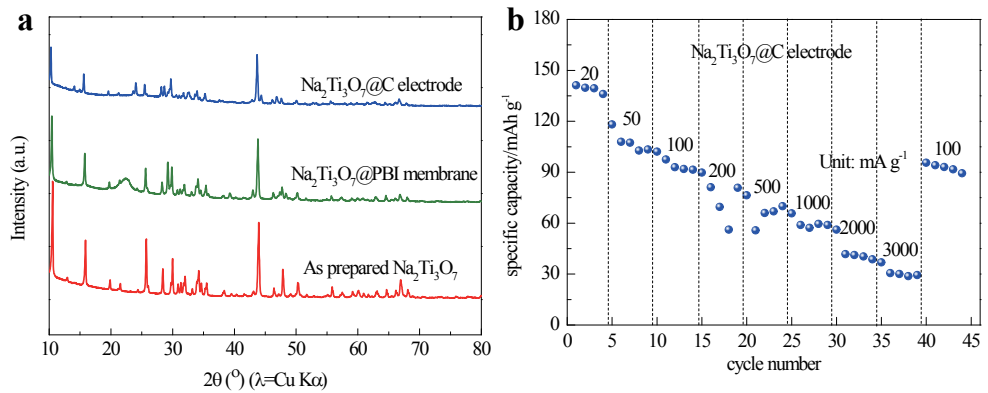


Figure S17. NaTi₃O₇@C electrode. (a) X-ray diffraction (XRD) patterns. (b) Rate capability.

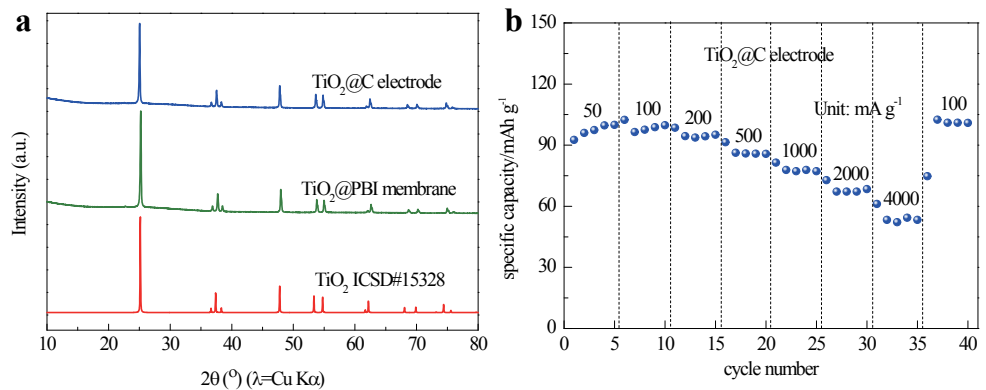


Figure S18. $\text{TiO}_2@\text{C}$ electrode. (a) X-ray diffraction (XRD) patterns. (b) Rate capability.

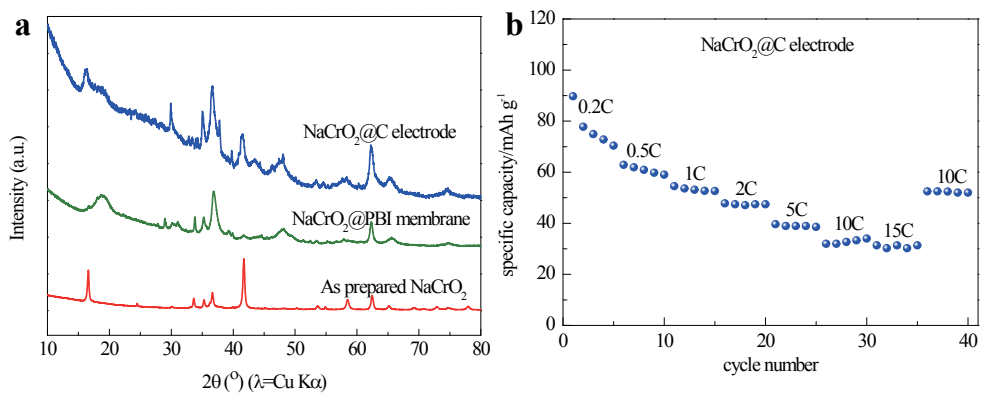


Figure S19. NaCrO₂@C electrode. (a) X-ray diffraction (XRD) patterns. (b) Rate capability.

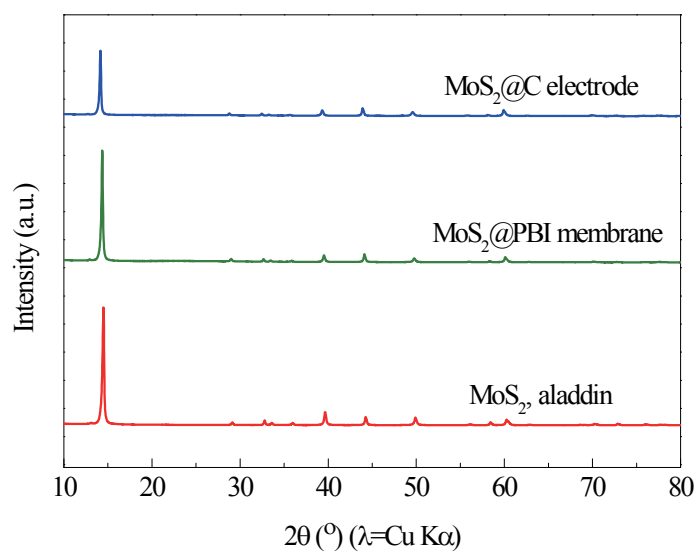


Figure S20. X-ray diffraction (XRD) patterns of MoS₂@C electrode.

Table S1 A comparison of present high-performance self-standing electrodes for sodium-ion batteries and this work.

Self-standing Materials	Synthesis methods	Initial Capacity	Rate capability	Cycle stability
Na ₃ V ₂ (PO ₄) ₃ @carbon fiber ¹	Electrospinning	77 mAh g ⁻¹ at 2 C	58 mAh g ⁻¹ at 5 C 20 mAh g ⁻¹ at 20 C	100% after 66 cycles at 2C
Na ₃ V ₂ (PO ₄) ₃ @carbon fiber ²	Electrospinning with insoluble precursor	116 mAh g ⁻¹ at 0.1 C	78 mAh g ⁻¹ at 10 C 63 mAh g ⁻¹ at 30 C	88.6% after 150 cycles at 0.5 C
Na ₃ V ₂ (PO ₄) ₃ /rGO paper ³	Annealing the peeled film	118 mAh g ⁻¹ at 50 mA g ⁻¹	104 mAh g ⁻¹ at 1000 mA g ⁻¹ 98 mAh g ⁻¹ at 2000 mA g ⁻¹	99.6% after 120 cycles at 100 mA g ⁻¹
NaVPO ₄ F@carbon fiber ⁴	Electrospinning	120 mAh g ⁻¹ at 1 C	101 mAh g ⁻¹ at 10 C 82 mAh g ⁻¹ at 30 C 61 mAh g ⁻¹ at 50 C	96.5% after 1000 cycles at 2 C
NaFePO ₄ @carbon fiber ⁵	Electrospinning	145 mAh g ⁻¹ at 0.2 C	84 mAh g ⁻¹ at 10 C 73 mAh g ⁻¹ at 20 C 61 mAh g ⁻¹ at 50 C	88% after 6300 cycles at 5 C
Na _{2/3} [Ni _{1/3} Mn _{2/3}]O ₂ /rGO ⁶	Vacuum filtration	86 mAh g ⁻¹ at 0.1 C	66 mAh g ⁻¹ at 6 C 59 mAh g ⁻¹ at 10 C	93% after 200 cycles at 1 C
Sn@carbon fiber ⁷	Electrospinning	633 mAh g ⁻¹ at 200 mA g ⁻¹	500 mAh g ⁻¹ at 5000 mA g ⁻¹ 450 mAh g ⁻¹ at 10000 mA g ⁻¹	90% after 1300 cycles at 2000 mA g ⁻¹
MoS ₂ @carbon fiber ⁸	Electrospinning	854 mAh g ⁻¹ at 100 mA g ⁻¹	623 mAh g ⁻¹ at 1000 mA g ⁻¹ 436 mAh g ⁻¹ at 5000 mA g ⁻¹	62% after 100 cycles at 1000 mA g ⁻¹
TiO ₂ Nanotube Arrays ⁹	Anodization method	322 mAh g ⁻¹ at 0.1 C	197 mAh g ⁻¹ at 5 C 167 mAh g ⁻¹ at 10 C	91% after 4400 cycles at 10 C
Na ₃ V ₂ (PO ₄) ₃ @porous carbon (This work)	Phase separation-derived method	110.4 mAh g ⁻¹ at 0.5 C	108.7 mAh g ⁻¹ at 5 C 108.2 mAh g ⁻¹ at 20 C 108.1 mAh g ⁻¹ at 40 C	90.4% after 2000 cycles at 1 C

References

- [1] J. Liu, K. Tang, K. Song, P. A. van Aken, Y. Yu and J. Maier, *Nanoscale* 2014, **6**, 5081.
- [2] Q. Ni, Y. Bai, Y. Li, L. Ling, L. Li, G. Chen, Z. Wang, H. Ren, F. Wu and C. Wu, *Small* 2018, **14**, 1702864.
- [3] W. Zhang, Y. Liu, C. Chen, Z. Li, Y. Huang and X. Hu, *Small* 2015, **11**, 3822.
- [4] T. Jin, Y. Liu, Y. Li, K. Cao, X. Wang and L. Jiao, *Adv. Energy Mater.* 2017, **7**, 1700087.
- [5] Y. Liu, N. Zhang, F. Wang, X. Liu, L. Jiao and L.-Z. Fan, *Adv. Funct. Mater.* 2018, **28**, 1801917.
- [6] D. Yang, X.-Z. Liao, J. Shen, Y.-S. He and Z.-F. Ma, *J. Mater. Chem. A* 2014, **2**, 6723.
- [7] Y. Liu, N. Zhang, L. Jiao and J. Chen, *Adv. Mater.* 2015, **27**, 6702.
- [8] C. Zhu, X. Mu, P. A. van Aken, Y. Yu and J. Maier, *Angew. Chem. Int. Ed.* 2014, **53**, 2152.
- [9] J. Ni, S. Fu, C. Wu, J. Maier, Y. Yu and L. Li, *Adv. Mater.* 2016, **28**, 2259.